Nuclear Engineering and Technology 49 (2017) 1645–1653

Contents lists available at ScienceDirect

Nuclear Engineering and Technology

journal homepage: www.elsevier.com/locate/net

Original Article

On the performance of heat absorption/generation and thermal stratification in mixed convective flow of an Oldroyd-B fluid

Tasawar Hayat [a, b], Muhammad Ijaz Khan [a, *], Muhammad Waqas [a], Ahmed Alsaedi [b]

[a] Department of Mathematics, Quaid-I-Azam University 45320, Islamabad 44000, Pakistan
[b] Nonlinear Analysis and Applied Mathematics (NAAM) Research Group, Department of Mathematics, Faculty of Science, King Abdulaziz University, P.O. Box 80257, Jeddah 21589, Saudi Arabia

ARTICLE INFO

Article history:
Received 7 June 2017
Received in revised form
11 July 2017
Accepted 25 July 2017
Available online 14 September 2017

Keywords:
Heat generation/absorption
Mixed convection
Oldroyd-B liquid
Stratification

ABSTRACT

This investigation explores the thermally stratified stretchable flow of an Oldroyd-B material bounded by a linear stretched surface. Heat transfer characteristics are addressed through thermal stratification and heat generation/absorption. Formulation is arranged for mixed convection. Application of suitable transformations provides ordinary differential systems through partial differential systems. The homotopy concept is adopted for the solution of nonlinear differential systems. The influence of several arising variables on velocity and temperature is addressed. Besides this, the rate of heat transfer is calculated and presented in tabular form. It is noticed that velocity and Nusselt number increase when the thermal buoyancy parameter is enhanced. Moreover, temperature is found to decrease for larger values of Prandtl number and heat absorption parameter. Comparative analysis for limiting study is performed and excellent agreement is found.

1. Introduction

Recent developments in advanced technologies have pushed several researchers to report liquid flows that demand communication of numerous phenomena. The understanding of mixed convective flows has recently improved because these flows are encountered frequently in both nature and in engineering equipment, for example, in the ocean, in certain features of electronic cooling, in nuclear reactor technology, and in the movement of flow in the atmosphere [1,2]. Stretched flows with mixed convection have been reported by several investigators. For example, mixed convective stretchable flow of a radiating Maxwell liquid was reported by Hayat et al. [3,4]. Shehzad et al. [5] explored mixed convection and magnetohydrodynamic (MHD) impact in the stretchable flow of a thixotropic liquid. Simultaneous characteristics of joule heating and MHD in nonlinear dissipative mixed convective flow of micropolar liquid were elucidated by Waqas et al. [6]. Furthermore, heat transfer characteristics regarding heat absorption or generation phenomenon have significance in industrial and engineering procedures such as dilution and strengthening of copper wires, fertilization, filled bed reactors, waste stowage materials, disassociating liquids, and several metallurgical procedures [7]. Several studies have been conducted on these phenomena [8–12].

The non-Newtonian materials are well recognized now in oil drilling, food processing biomechanics, plastic and paper making processes, and many other fields. These materials cannot be classified by one expression. Thus, several relations regarding non-Newtonian liquids have been presented [13–20]. In this work, we are interested in exploring the salient characteristics of Oldroyd-B liquid, which is a modified form of a Maxwell liquid that portrays the relaxation of stress through constant strain. However, memory impacts cannot be interpreted through Maxwell materials. Thus, to interpret the characteristics of memory and elasticity, the Oldroyd-B liquid model has been recommended. Several biological and polymeric materials are commonly used to illustrate the impacts of memory and elasticity. Moreover, this model is often used to report small relaxation/retardation times. In the absence of a retardation time factor, this model corresponds to the Maxwell liquid model. Also, the case of the classical Newtonian liquid model is recovered when relaxation/retardation factors are absent. Several investigations into the Oldroyd-B liquid model have been reported [21–26].

The abovementioned attempts clearly reveal that the aspect of thermal stratification has not been properly addressed. This aspect arises owing to the temperature difference, which gives rise to density variation in the medium. Examples of thermal stratification

* Corresponding author.
E-mail address: ijazfmg_khan@yahoo.com (M.I. Khan).

https://doi.org/10.1016/j.net.2017.07.027

include lake thermohydraulics, geothermal systems, power plant contraction systems, geological transport, and volcanic flows. Kandasamy et al. [27] addressed the thermally stratified stretchable flow of magneto viscous nanoliquid by considering solar radiation. Cross diffusion and MHD aspects in dissipative stratified flow of viscous liquid were explored by Zaib and Shafie [28]. Hayat et al. [29,30] examined the thermal stratification characteristics in stretchable flows of Eyring–Powell and Jeffrey materials. Several investigations have already been conducted on heat transfer [31–33].

Keeping the abovementioned investigations in view, the intention of the current attempt is fourfold. First, to model and investigate the two-dimensional (2-D) flow of an Oldroyd-B liquid bounded by a linear stretchable surface; second, to report on the mixed convection aspect; third, to consider the effects of heat absorption/generation and thermal stratification; and fourth, using the homotopy scheme, to derive convergent series solutions for the velocity and temperature [34–44]. The contributions of the arising physical variables are interpreted and discussed in detail. Furthermore, the heat transfer rate has also been analyzed via numerical values.

2. Formulation

Here, the 2-D mixed convective flow of an incompressible Oldroyd-B liquid bounded by a linear stretchable surface is investigated. The sheet has linear velocity of $u_w(x) = cx$, where c denotes the stretching rate. Heat transfer in the presence of heat generation/absorption and thermal stratification is reported. The boundary layer concept is adopted for the whole treatment. With these assumptions in view, the continuity, momentum, and energy relations governing the flow are:

$$\frac{\partial u}{\partial x} + \frac{\partial v}{\partial y} = 0, \tag{1}$$

$$u\frac{\partial u}{\partial x} + v\frac{\partial u}{\partial y} + \lambda_1\left(u^2\frac{\partial^2 u}{\partial x^2} + v^2\frac{\partial^2 u}{\partial y^2} + 2uv\frac{\partial^2 u}{\partial x \partial y}\right) = \nu\left[\frac{\partial^2 u}{\partial y^2} + \lambda_2\left(u\frac{\partial^3 u}{\partial x \partial y^2} + v\frac{\partial^3 u}{\partial y^3} - \frac{\partial u}{\partial x}\frac{\partial^2 u}{\partial y^2} - \frac{\partial u}{\partial y}\frac{\partial^2 v}{\partial y^2}\right)\right] + g\beta_T(T - T_\infty), \tag{2}$$

$$u\frac{\partial T}{\partial x} + v\frac{\partial T}{\partial y} = \alpha\frac{\partial^2 T}{\partial y^2} + \frac{Q_0}{\rho c_p}(T - T_\infty), \tag{3}$$

subjected to the conditions

$$\begin{aligned} &u = u_w(x) = cx,\ \ v = 0,\ \ T = T_w = T_0 + ax \text{ at } y = 0,\\ &u \to 0,\ \ T \to T_\infty = T_0 + bx \text{ as } y \to \infty. \end{aligned} \tag{4}$$

Here, the velocity components are denoted by $(u,\ v)$ in (x,y) directions, respectively, with ν standing for kinematic viscosity, ρ for liquid density, c_p for specific heat, $(\lambda_1,\ \lambda_2)$ for relaxation/retardation times, g for gravitational acceleration, β_T for thermal expansion coefficient, $\alpha = \left(\frac{k}{\rho c_p}\right)$ for the thermal diffusivity, k for the thermal conductivity, Q_0 for the uniform volumetric heat absorption/generation coefficient, $(T,\ T_\infty)$ for the fluid and ambient fluid temperatures, T_0 for the reference temperature, and $(a,\ b)$ for the dimensional constants.

The following variables are used in order to transform Eqs. (2–4) into a system of dimensionless expressions:

$$\eta = y\sqrt{\frac{c}{\nu}},\ \ u = cxf'(\eta),\ \ v = -\sqrt{c\nu}f(\eta),\ \ \theta(\eta) = \frac{T - T_\infty}{T_w - T_0}. \tag{5}$$

The continuity expression is fulfilled identically and remaining expressions [i.e., (2)–(4)] have the final forms:

$$f''' + ff'' - f'^2 + \beta_1\left(2ff'f'' - f^2f'''\right) + \beta_2\left(f''^2 - ff^{iv}\right) + \lambda\theta = 0, \tag{6}$$

$$\theta'' + Pr(f\theta' - f'\theta) - PrSf' + Pr\delta\theta = 0, \tag{7}$$

$$\begin{aligned} &f = 0,\ \ f' = 1,\ \ \theta = 1 - S \text{ at } \eta = 0,\\ &f' \to 0,\ \ \theta \to 0 \text{ as } \eta \to \infty. \end{aligned} \tag{8}$$

Here, $(\beta_1,\ \beta_2)$ represents the Deborah numbers, λ the mixed convection or thermal buoyancy parameter, Gr_x the Grashof number due to temperature, Re_x the local Reynolds number, Pr the Prandtl number, S the thermal stratified parameter, and δ the heat generation (>0) and absorption (<0). The results for viscous fluid are obtained when $\beta_1 = \beta_1 = 0$. These parameters have the following definitions:

$$\beta_1 = \lambda_1 c,\ \ \beta_2 = \lambda_2 c,\ \ \lambda = \frac{Gr_x}{Re_x^2} = \frac{g\beta_T a}{c^2},\ \ Gr_x = \frac{g\beta_T(T_w - T_0)\,x^3}{\nu^2},$$
$$Re_x = \frac{xu_w(x)}{\nu},\ \ Pr = \frac{\nu}{\alpha},\ \ S = \frac{b}{a},\ \ \delta = \frac{Q_0}{\rho c_p c}. \tag{9}$$

The local Nusselt number Nu_x is expressed as:

$$Nu_x = \frac{xq_w}{k(T_w - T_0)},\ \ q_w = -k\left(\frac{\partial T}{\partial y}\right)\bigg|_{y=0}. \tag{10}$$

In non-dimensional variables, we have

$$Nu_x Re_x^{-1/2} = -\theta'(0). \tag{11}$$

3. Series solutions

To calculate series solutions of Expressions (6) and (7), we used the homotopic technique [34–44]. We have the following initial guesses and auxiliary linear operators:

$$f_0(\eta) = 1 - e^{-\eta},\ \ \theta_0(\eta) = (1 - S)\exp(-\eta), \tag{12}$$

$$L_f = f''' - f',\ \ L_\theta = \theta'' - \theta. \tag{13}$$

The abovementioned auxiliary linear operators must validate the following properties:

$$\left.\begin{aligned} &L_f\left(C_1 + C_2e^{\eta} + C_3e^{-\eta}\right) = 0,\\ &L_\theta\left(C_4e^{\eta} + C_5e^{-\eta}\right) = 0, \end{aligned}\right\} \tag{14}$$

where $C_i\ \ (i = 1 - 5)$ indicate the arbitrary constants.

The corresponding problems at the zeroth order are represented as follows:

$$(1 - p)L_f\left[\hat{f}(\eta;\ p) - f_0(\eta)\right] = p\hbar_f\mathbf{N}_f\left[\hat{f}(\eta;\ p),\ \hat{\theta}(\eta,\ p)\right], \tag{15}$$

$$(1 - p)L_\theta\left[\hat{\theta}(\eta;\ p) - \theta(\eta)\right] = p\hbar_\theta\mathbf{N}_\theta\left[\hat{f}(\eta;\ p),\ \hat{\theta}(\eta,\ p)\right], \tag{16}$$

$$\widehat{f}(0;\ p)=0,\ \widehat{f}'(0;\ p)=1,\ \widehat{f}'(\infty;\ p)=0,\ \widehat{\theta}(0,\ p)=1-S,\ \widehat{\theta}(\infty,\ p)=0, \tag{17}$$

$$\begin{aligned}\mathbf{N}_f\left[\widehat{f}(\eta;\ p)\right]=&\frac{\partial^3\widehat{f}(\eta;\ p)}{\partial\eta^3}+\widehat{f}(\eta;\ p)\frac{\partial^2\widehat{f}(\eta;\ p)}{\partial\eta^2}-\left(\frac{\partial\widehat{f}(\eta;\ p)}{\partial\eta}\right)^2\\&+\beta_1\left[2\widehat{f}(\eta;\ p)\frac{\partial\widehat{f}(\eta;\ p)}{\partial\eta}\frac{\partial^2\widehat{f}(\eta;\ p)}{\partial\eta^2}-\left(\widehat{f}(\eta;\ p)\right)^2\frac{\partial^3\widehat{f}(\eta;\ p)}{\partial\eta^3}\right]+\beta_2\left[\left(\frac{\partial^2\widehat{f}(\eta;\ p)}{\partial\eta^2}\right)^2\right.\\&\left.-\widehat{f}(\eta;\ p)\frac{\partial^4\widehat{f}(\eta;\ p)}{\partial\eta^4}\right]+\lambda\widehat{\theta}(\eta;\ p),\end{aligned} \tag{18}$$

$$\begin{aligned}\mathbf{N}_\theta\left[\widehat{f}(\eta;p),\widehat{\theta}(\eta;p)\right]=&\frac{\partial^2\widehat{\theta}(\eta;p)}{\partial\eta^2}+Pr\left(\widehat{f}(\eta;p)\frac{\partial\widehat{\theta}(\eta;p)}{\partial\eta}-\frac{\partial\widehat{f}(\eta;p)}{\partial\eta}\widehat{\theta}(\eta;p)\right)-PrS\frac{\partial\widehat{f}(\eta;p)}{\partial\eta}\\&+Pr\delta\widehat{\theta}(\eta;p).\end{aligned} \tag{19}$$

here, the embedding parameter is represented by p and the nonzero auxiliary parameters are denoted by $(\hbar_f,\hbar_\theta)$.

The developed problems at the m^{th}-order deformation are formulated in the forms:

$$L_f[f_m(\eta)-\chi_m f_{m-1}(\eta)]=\hbar_f\mathbf{R}_f^m(\eta), \tag{20}$$

$$L_\theta[\theta_m(\eta)-\chi_m\theta_{m-1}(\eta)]=\hbar_\theta\mathbf{R}_\theta^m(\eta), \tag{21}$$

$$f_m(0)=f'_m(0)=f'_m(\infty)=0,\ \ \theta_m(0)=\theta_m(\infty)=0, \tag{22}$$

$$\begin{aligned}\mathbf{R}_f^m(\eta)=&f'''_{m-1}(\eta)+\sum_{k=0}^{m-1}(f_{m-1-k}f''_k-f'_{m-1-k}f'_k)\\&+\beta_1\sum_{k=0}^{m-1}\left(2f_{m-1-k}\sum_{l=0}^{k}f'_{k-l}f''_l-f_{m-1-k}\sum_{l=0}^{k}f_{k-l}f''_l\right)\\&+\beta_2\left(f''_{m-1-k}\sum_{k=0}^{m-1}f''_k-f_{m-1-k}\sum_{k=0}^{m-1}f''''_k\right)+\lambda\theta_{m-1}(\eta),\end{aligned} \tag{23}$$

$$\mathbf{R}_\theta^m(\eta)=\theta''_{m-1}(\eta)+Pr\sum_{k=0}^{m-1}(\theta'_{m-1-k}f_k-\theta_{m-1-k}f'_k)-PrSf'_{m-1}(\eta)+Pr\delta\theta_{m-1}(\eta), \tag{24}$$

$$\chi_m=\begin{cases}0, & m\le 1,\\ 1, & m>1.\end{cases} \tag{25}$$

The general solution expressions now are:

$$f_m(\eta)=f_m^*(\eta)+C_1+C_2e^{\eta}+C_3e^{-\eta}, \tag{26}$$

$$\theta_m(\eta)=\theta_m^*(\eta)+C_4e^{\eta}+C_5e^{-\eta}, \tag{27}$$

here, special solutions are denoted by f_m^* and θ_m^*.

4. Convergence analysis

This section aims to certify the convergence of Expressions (20) and (21) subject to the boundary conditions of Expression (22). Clearly, Expressions (20) and (21) comprise auxiliary variables $(\hbar_f,\hbar_\theta)$. These variables are used to control and adjust the convergence region. Hence, we show the $\hbar$ curves in Fig. 1. Allowable values for established solutions are in the ranges of $-1.95\le\hbar_f\le-0.25$ and $-2.00\le\hbar_\theta\le-0.35$. Table 1 shows the convergence through numerical values. Clearly, 15^{th}-order approximations are sufficient for the convergence of the momentum and energy expressions.

5. Discussion

In this segment, physical illustrations of distinct variables such as the velocity $f'(\eta)$ and temperature $\theta(\eta)$ distribution are presented in Figs. 2–9. The impact of β_1 on $f'(\eta)$ is illustrated in Fig. 2. Clearly, $f'(\eta)$ and the thickness of the momentum boundary layer are decaying functions of the larger Deborah number (β_1) because β_1 arises owing to the relaxation time factor. A larger β_1 corresponds to a longer relaxation time factor, and this factor resists the liquid flow owing to the lower velocity and thinner momentum layer. Moreover, an increment in β_2 provides an improvement in $f'(\eta)$, and in the thickness of the momentum boundary layer (for details, see Fig. 3). Actually, the Deborah number (β_2) is directly associated with the retardation time factor; this factor has the ability to improve the liquid velocity. It is worth mentioning that the case of Maxwell liquid flow is achieved by letting $\beta_2=0$. Also, the case of a viscous liquid can be obtained by setting $\beta_1=\beta_2=0$. Fig. 4 shows the effects of λ on $f'(\eta)$. Here, both f' and the corresponding thickness layer increase when λ increases because λ yields higher buoyancy forces, which correspond to higher velocity. The effects of Pr on temperature (θ) are reported in Fig. 5. It should be noticed that the rise in Pr corresponds to decays in the temperature (θ) and thickness of the thermal boundary layer because Pr is the ratio of momentum to thermal diffusivity. For larger Pr, the thermal diffusivity is lower because the diffusion rate drops. This drop in the rate of diffusion acts as a representative exhibiting a diminution in temperature (θ) and thickness of thermal layer. The appropriate Prandtl numbers are reasonably important in industrial procedures because they are used to control the rate of heat transfer in the ultimate product. Fig. 6 illustrates the effect of S on $\theta(\eta)$. Here, θ is lower for higher values of S. In fact, the temperature difference steadily drops between the surface of the sheet and the ambient liquid; this reduction produces a drop in temperature (θ). The effects of $\delta>0$ and $\delta<0$ on temperature (θ) are illustrated in Figs. 7 and 8, respectively. Here, $\theta(\eta)$ is an increasing function of $\delta>0$, whereas the opposite situation is noticed for $\delta<0$. Physically, heat transfers significantly at larger δ, which corresponds to higher temperature (θ) when compared with $\delta<0$. Thus temperature (θ) increases via $\delta>0$ and drops for $\delta<0$. Fig. 9 shows the effect of λ on temperature (θ). As expected, temperature (θ) and thickness of the thermal layer drop with an increase in λ. Physically, buoyancy force controls the inertial force, which improves the heat transfer rate. Consequently, the temperature (θ) drops.

Impacts of distinct variables on the Nusselt number $(Nu_xRe_x^{-1/2})$ are shown in Table 2. Clearly, Nusselt number increases with larger Pr and λ, whereas the reverse behavior is found in the cases of δ and S. Table 3 provides a comparative analysis of the results provided in two studies [45,46]. It is concluded that our series expressions are in reasonable agreement with those of Abel et al. [45] and Megahed [46]. Table 4 validates the presented analysis according to the results of the studies provided by Sadeghy et al. [47] and Mukhopadhyay [48]. In this table, it can also be noticed that the analytical expressions we present are in excellent agreement with those in

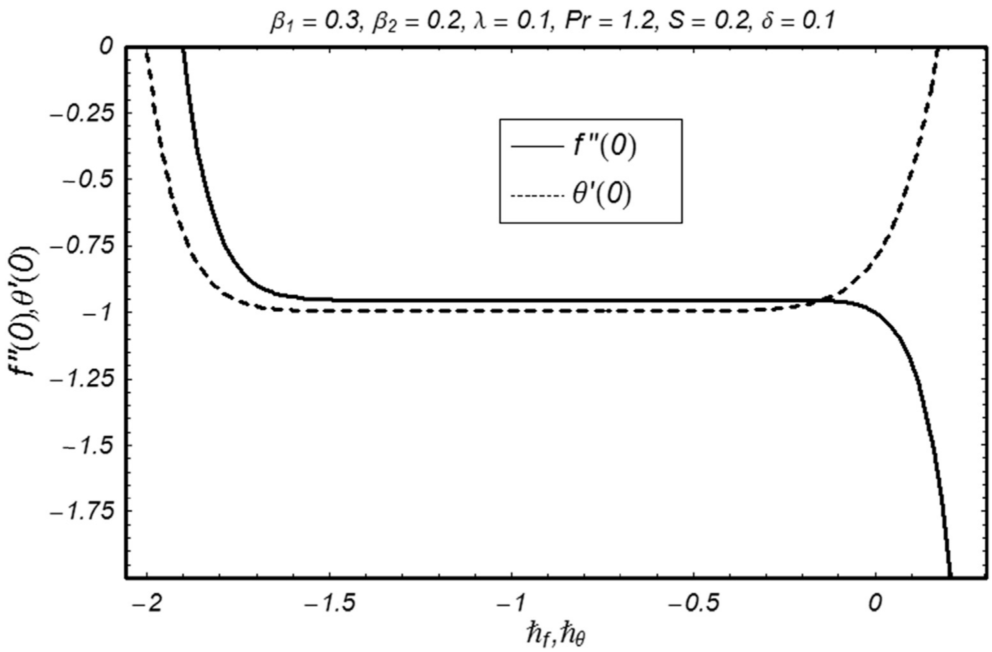

Fig. 1. ħ curves for f and θ.

Table 1
Homotopy solution convergence when $\beta_1 = 0.3$, $\beta_2 = S = 0.2$, $\lambda = \delta = 0.1$, and $Pr = 1.2$.

Order of approximations	$-f''(0)$	$-\theta'(0)$
1	0.9350	0.9520
5	0.9544	0.9957
10	0.9545	0.9958
15	0.9545	0.9958
20	0.9545	0.9958
25	0.9545	0.9958
30	0.9545	0.9958

the studies by Sadeghy et al. [47] and Mukhopadhyay [48]. Moreover, it should be noticed that the numerical values of $f''(0)$ are higher for larger β_1 because the Deborah number (β_1) is directly proportional to the relaxation time factor (λ_1). The value of λ_1 increases with higher β_1. Thus, a higher relaxation time decays the liquid velocity but increases $f''(0)$.

6. Concluding remarks

In this study, computations are presented to explore the 2-D stretchable mixed convective flow of an Oldroyd-B material in the

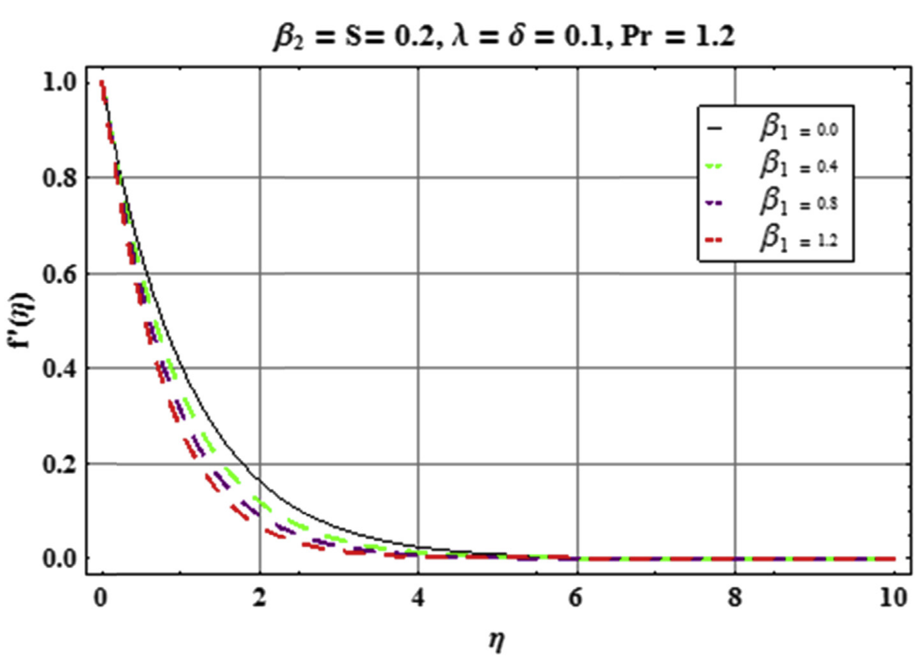

Fig. 2. f' via β_1.

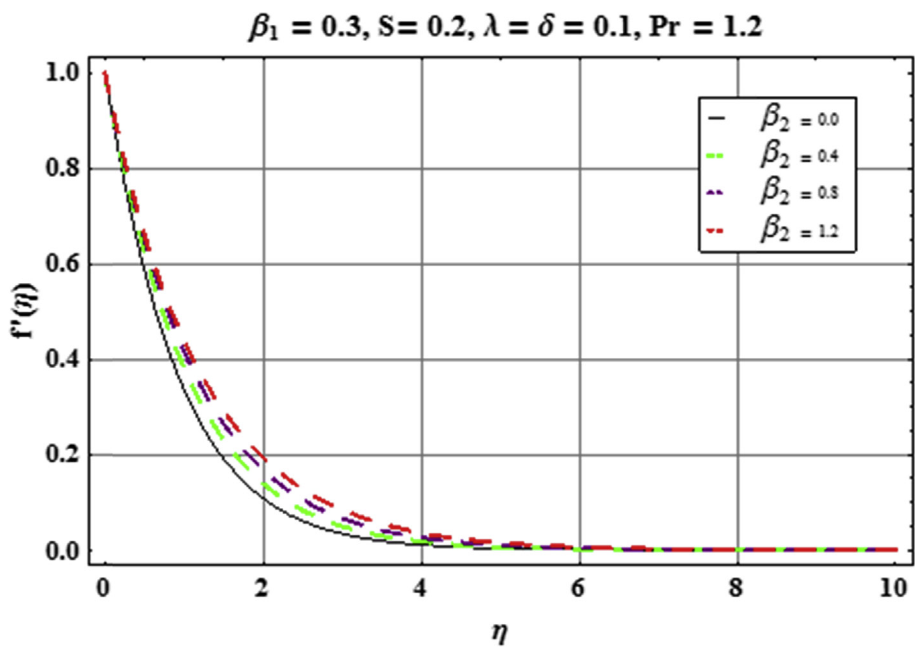

Fig. 3. f' via β_2.

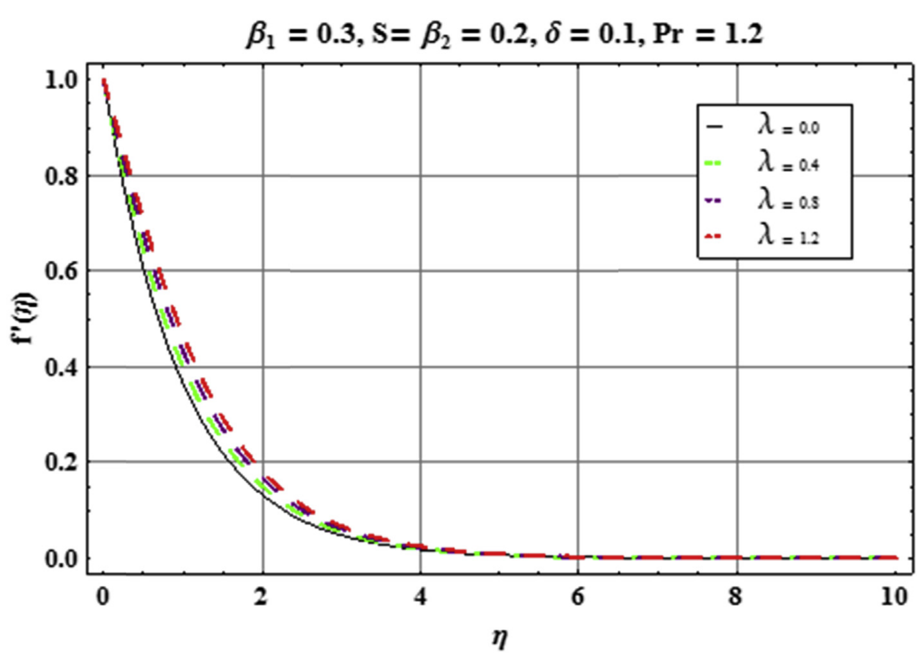

Fig. 4. f' via λ.

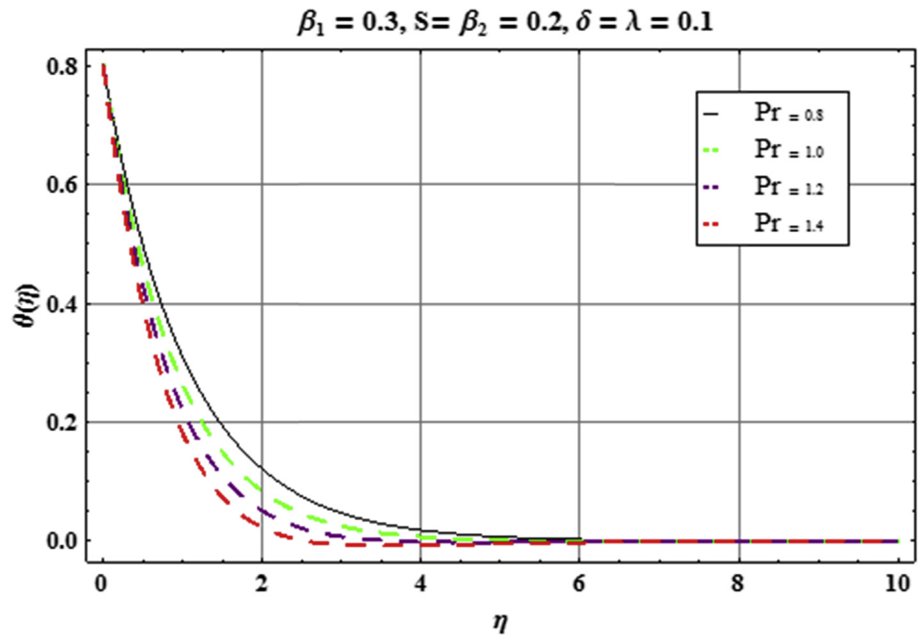

Fig. 5. θ via *Pr*.

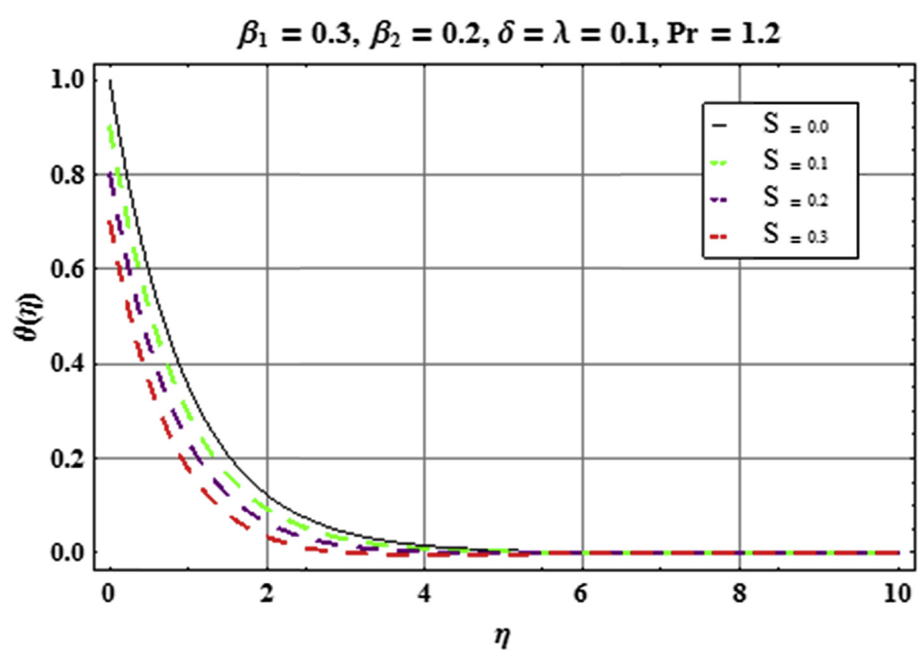

Fig. 6. θ via *S*.

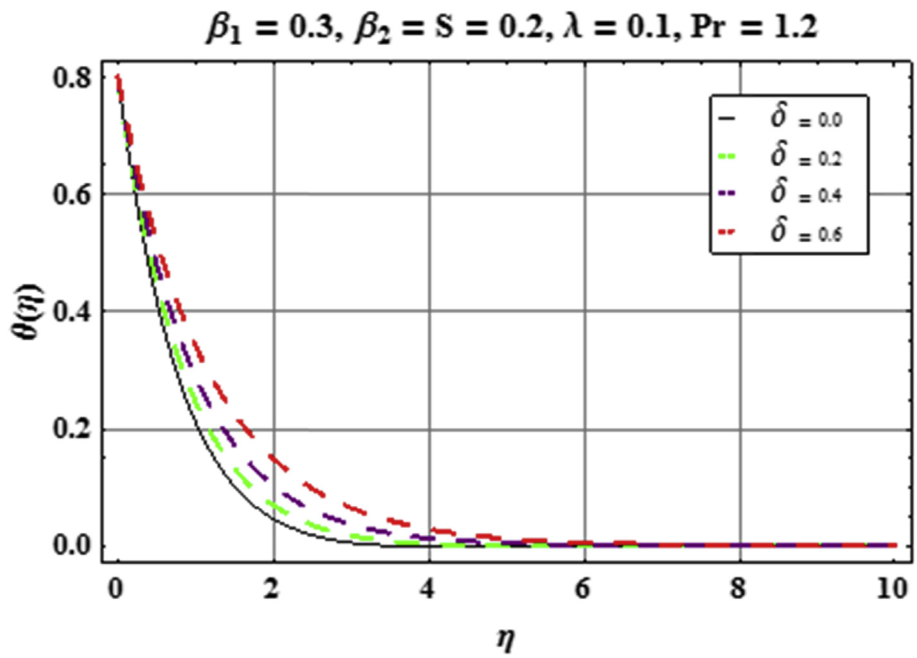

Fig. 7. θ via $\delta > 0$.

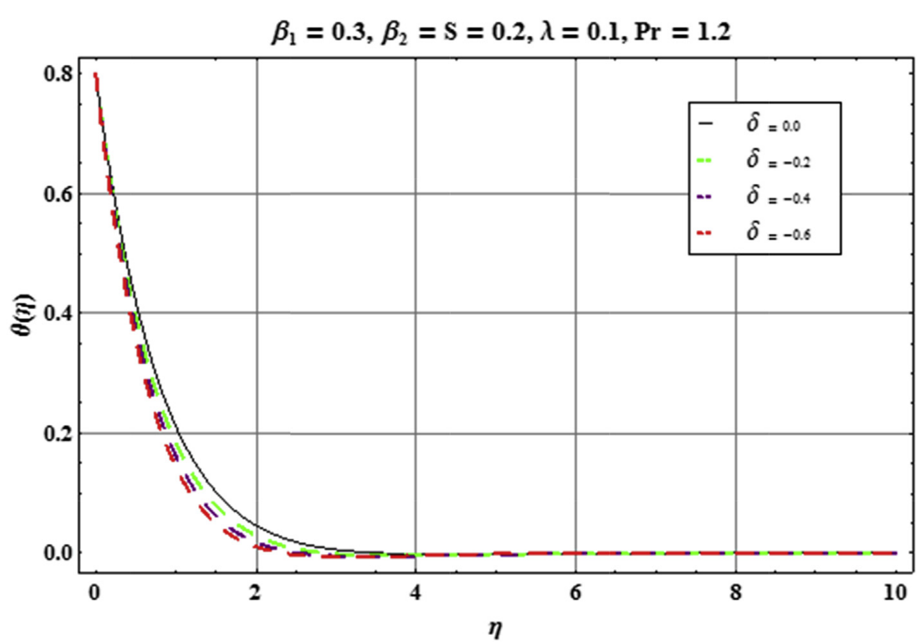

Fig. 8. θ via $\delta < 0$.

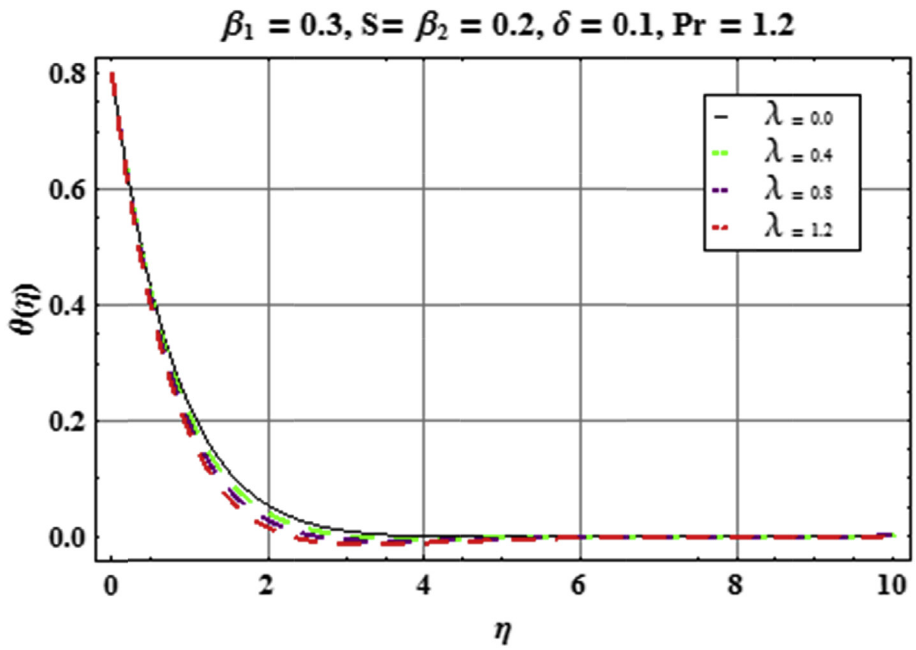

Fig. 9. θ via λ.

Table 2
Behaviors of δ, S, Pr, and λ on Nusselt number $(Nu_x Re_x^{-1/2})$ when $\beta_1 = 0.3$ and $\beta_2 = 0.2$.

δ	S	Pr	λ	$-\theta'(0)$
0.0	0.2	1.2	0.1	1.0033
0.2				0.8921
0.3				0.8147
0.1	0.0			1.0165
	0.3			0.9185
	0.6			0.8165
	0.2	1.3		1.0044
		1.4		1.0554
		1.5		1.1048
		1.2	0.0	0.9407
			0.2	0.9608
			0.4	0.9764

Table 3
Comparison of numerical values of $f''(0)$ with those in the studies by Abel et al. [45] and Megahed [46] for several values of β_1 when $\beta_2 = 0 = \lambda$.

β_1	Abel et al. [45]	Megahed [46]	Present
0.0	1.000000	0.999978	1.000000
0.2	1.051948	1.051945	1.051889
0.4	1.101850	1.101848	1.101903
0.6	1.150163	1.150160	1.150137
0.8	1.196692	1.196690	1.196711
1.2	1.285257	1.285253	1.285363
1.6	1.368641	1.368641	1.368758
2.0	1.447617	1.447616	1.447651

Table 4
Comparative analysis of $f''(0)$ with the studies by Sadeghy et al. [47] and Mukhopadhyay [48] for distinct values of β_1 when $\beta_2 = 0 = \lambda$.

β_1	Sadeghy et al. [47]	Mukhopadhyay [48]	Present
0.0	1.000000	0.9999963	1.000000
0.2	1.0594	1.051949	1.051889
0.4	1.10084	1.101851	1.101903
0.6	1.0015016	1.150162	1.150137
0.8	1.19872	1.196693	1.196711

presence of heat generation/absorption and thermal stratification. The present analysis has the following outcomes: (1) larger β_1 retards the flow, whereas the reverse situation is noticed for β_2; (2) thermal buoyancy or mixed convection parameter (λ) shows opposite behaviors on velocity and temperature; (3) larger Pr corresponds to a decay in the temperature profile (θ) and in the thickness of the thermal boundary layer; (4) heat transfers more rapidly in the case of the heat generation process ($\delta > 0$); however, it is absorbed when ($\delta < 0$); (5) Nusselt number increases when Pr and λ are increased, whereas it decays via larger S and δ; and (6) the case of no heat generation/absorption can be achieved by setting $\delta = 0$.

Conflict of interest

It is declared that authors have no conflict of interest.

References

[1] M. Fakour, A. Vahabzadeh, D.D. Ganji, Scrutiny of mixed convection flow of a nanofluid in a vertical channel, Case Stud. Therm. Eng. 4 (2014) 15–23.
[2] N.A. Othman, N.A. Yacob, N. Bachok, A. Ishak, I. Pop, Mixed convection boundary-layer stagnation point flow past a vertical stretching/shrinking surface in a nanofluid, Appl. Thermal Eng. 115 (2017) 1412–1417.
[3] T. Hayat, M. Waqas, S.A. Shehzad, A. Alsaedi, Mixed convection radiative flow of Maxwell fluid near a stagnation point with convective condition, J. Mech. 29 (2013) 403–409.
[4] T. Hayat, M. Waqas, S.A. Shehzad, A. Alsaedi, Effects of Joule heating and thermophoresis on stretched flow with convective boundary conditions, Sci. Iran. B 21 (2014) 682–692.
[5] S.A. Shehzad, F.E. Alsaadi, T. Hayat, S.J. Monaquel, MHD mixed convection flow of thixotropic fluid with thermal radiation, ASME Heat Transfer Res. 45 (2014) 569–576.
[6] M. Waqas, M. Farooq, M.I. Khan, A. Alsaedi, T. Hayat, T. Yasmeen, Magnetohydrodynamic (MHD) mixed convection flow of micropolar liquid due to nonlinear stretched sheet with convective condition, Int. J. Heat Mass Transfer 102 (2016) 766–772.
[7] T. Hayat, S. Qayyum, S.A. Shehzad, A. Alsaedi, Magnetohydrodynamic three-dimensional nonlinear convection flow of Oldroyd-B nanoliquid with heat generation/absorption, J. Mol. Liq. 230 (2017) 641–651.
[8] W.A. Khan, M. Khan, R. Malik, Three-dimensional flow of an Oldroyd-B nanofluid towards stretching surface with heat generation/absorption, PLoS One 9 (2014), e105107.

[9] T. Hayat, S. Ali, M.A. Farooq, A. Alsaedi, On comparison of series and numerical solutions for flow of Eyring–Powell fluid with Newtonian heating and internal heat generation/absorption, PLoS One 10 (2015), e0129613.
[10] T. Hayat, F. Shah, A. Alsaedi, M.I. Khan, Development of homogeneous/heterogeneous reaction in flow based through non-Darcy Forchheimer medium, J. Theor. Comput. Chem. 16 (2017), 1750045.
[11] B. Mahanthesh, B.J. Gireesha, R.S.R. Gorla, Heat and mass transfer effects on the mixed convective flow of chemically reacting nanofluid past a moving/stationary vertical plate, Alex. Eng. J. 55 (2016) 569–581.
[12] T. Hayat, M. Waqas, M.I. Khan, A. Alsaedi, Impacts of constructive and destructive chemical reactions in magnetohydrodynamic (MHD) flow of Jeffrey liquid due to nonlinear radially stretched surface, J. Mol. Liq. 225 (2017) 302–310.
[13] T. Hayat, M. Sajid, I. Pop, Three-dimensional flow over a stretching surface in a viscoelastic fluid, Nonlinear Anal. Real World Appl. 9 (2008) 1811–1822.
[14] T. Hayat, N. Ahmed, M. Sajid, S. Asghar, On the MHD flow of a second grade fluid in a porous channel, Comput. Math. Appl. 54 (2007) 407–414.
[15] M.I. Khan, M. Waqas, T. Hayat, A. Alsaedi, A comparative study of Casson fluid with homogeneous–heterogeneous reactions, J. Colloid Interface Sci. 498 (2017) 85–90.
[16] N. Ali, T. Hayat, S. Asghar, Peristaltic flow of a Maxwell fluid in a channel with compliant walls, Chaos Solitons Fractals 39 (2009) 407–416.
[17] T. Hayat, M. Khan, M. Ayub, Exact solutions of flow problems of an Oldroyd-B fluid, Appl. Math. Comput. 151 (2004) 105–119.
[18] R. Ellahi, E. Shivanian, S. Abbasbandy, T. Hayat, Analysis of some magnetohydrodynamic flows of third-order fluid saturating porous space, J. Porous Media 18 (2015) 89–98.
[19] M. Turkyilmazoglu, Dual and triple solutions for MHD slip flow of non-Newtonian fluid over a shrinking surface, Comput. Fluid 70 (2012) 53–58.
[20] M.I. Khan, T. Hayat, M. Waqas, A. Alsaedi, Outcome for chemically reactive aspect in flow of tangent hyperbolic material, J. Mol. Liq. 230 (2017) 143–151.
[21] M. Anand, J. Kwack, A. Masud, A new generalized Oldroyd-B model for blood flow in complex geometries, Int. J. Eng. Sci. 72 (2013) 78–88.
[22] T. Hayat, M.I. Khan, M. Farooq, A. Alsaedi, M. Waqas, T. Yasmeen, Impact of Cattaneo–Christov heat flux model in flow of variable thermal conductivity fluid over a variable thicked surface, Int. J. Heat Mass Transfer 99 (2016) 702–710.
[23] M. Sajid, B. Ahmed, Z. Abbas, Steady mixed convection stagnation point flow of MHD Oldroyd-B fluid over a stretching sheet, J. Egypt. Math. Soc. 23 (2015) 440–444.
[24] T. Hayat, M. Waqas, S.A. Shehzad, A. Alsaedi, On 2D stratified flow of an Oldroyd-B fluid with chemical reaction: an application of non-Fourier heat flux theory, J. Mol. Liq. 223 (2016) 566–571.
[25] S.S. Motsa, Z.G. Makukula, S. Shateyi, Numerical investigation of the effect of unsteadiness on three-dimensional flow of an Oldroyd-B fluid, PLoS One 10 (2015), e0133507.
[26] T. Hayat, S. Farooq, A. Alsaedi, B. Ahmad, Numerical study for Soret and Dufour effects on mixed convective peristalsis of Oldroyd 8-constants fluid, Int. J. Thermal Sci. 112 (2017) 68–81.
[27] R. Kandasamy, I. Muhaimin, R. Mohamad, Thermophoresis and Brownian motion effects on MHD boundary-layer flow of a nanofluid in the presence of thermal stratification due to solar radiation, Int. J. Mech. Sci. 70 (2013) 146–154.
[28] A. Zaib, S. Shafie, Thermal diffusion and diffusion thermo effects on unsteady MHD free convection flow over a stretching surface considering Joule heating and viscous dissipation with thermal stratification, chemical reaction and Hall current, J. Franklin Inst. 351 (2014) 1268–1287.
[29] T. Hayat, M. Zubair, M. Ayub, M. Waqas, A. Alsaedi, Stagnation point flow towards nonlinear stretching surface with Cattaneo–Christov heat flux, Eur. Phys. J. Plus 131 (2016) 355.
[30] T. Hayat, M.I. Khan, M. Farooq, A. Alsaedi, M.I. Khan, Thermally stratified stretching flow with Cattaneo–Christov heat flux, Int. J. Heat Mass Transfer 106 (2017) 289–294.
[31] M. Mamourian, K.M. Shirvan, R. Ellahi, A.B. Rahimi, Optimization of mixed convection heat transfer with entropy generation in a wavy surface square lid-driven cavity by means of Taguchi approach, Int. J. Heat Mass Transfer 102 (2016) 544–554.
[32] R. Ellahi, M. Hassan, A. Zeeshan, Aggregation effects on water base Al_2O_3-nanofluid over permeable wedge in mixed convection, Asia-Pac. J. Chem. Eng. 11 (2016) 179–186.
[33] R. Ellahi, M. Hassan, A. Zeeshan, A.A. Khan, The shape effects of nanoparticles suspended in HFE-7100 over wedge with entropy generation and mixed convection, Appl. Nanosci 6 (2016) 641–651.
[34] S.J. Liao, Homotopic Analysis Method in Nonlinear Differential Equations, Springer, Heidelberg, Germany, 2012.
[35] T. Hayat, S. Qayyum, M. Imtiaz, A. Alsaedi, Impact of Cattaneo–Christov heat flux in Jeffrey fluid flow with homogeneous–heterogeneous reactions, PLoS One 11 (2016), e0148662.
[36] T. Hayat, M.I. Khan, M. Farooq, T. Yasmeen, A. Alsaedi, Stagnation point flow with Cattaneo–Christov heat flux and homogeneous–heterogeneous reactions, J. Mol. Liq. 220 (2016) 49–55.
[37] M.I. Khan, T. Hayat, M.I. Khan, A. Alsaedi, A modified homogeneous–heterogeneous reactions for MHD stagnation flow with viscous dissipation and Joule heating, Int. J. Heat Mass Transfer 113 (2017) 310–317.
[38] J. Sui, L. Zheng, X. Zhang, Boundary layer heat and mass transfer with Cattaneo–Christov double-diffusion in upper-convected Maxwell nanofluid past a stretching sheet with slip velocity, Int. J. Thermal Sci. 104 (2016) 461–468.
[39] M.I. Khan, M. Waqas, T. Hayat, A. Alsaedi, Magnetohydrodynamic (MHD) stagnation point flow of Casson fluid over a stretched surface with homogeneous–heterogeneous reactions, J. Theor. Comput. Chem. 16 (2017), 1750022.
[40] T. Hayat, M.I. Khan, M. Waqas, M.I. Khan, A. Alsaedi, Radiative flow of micropolar nanofluid accounting thermophoresis and Brownian moment, Int. J. Hydrogen Energy 42 (2017) 16821–16833.
[41] T. Hayat, M.I. Khan, M. Imtiaz, A. Alsaedi, Heat and mass transfer analysis in the stagnation region of Maxwell fluid with chemical reaction over a stretched surface, J. Thermal Sci. Eng. Appl. 10 (2017), 011002.
[42] M.I. Khan, M.I. Khan, M. Waqas, T. Hayat, A. Alsaedi, Chemically reactive flow of Maxwell liquid due to variable thicked surface, Int. Commun. Heat Mass Transfer 86 (2017) 231–238.
[43] M.W.A. Khan, M. Waqas, M.I. Khan, A. Alsaedi, T. Hayat, MHD stagnation point flow accounting variable thickness and slip conditions, Colloid Polym. Sci. 295 (2017) 1201–1209.
[44] M.I. Khan, M. Waqas, T. Hayat, M.I. Khan, A. Alsaedi, Behavior of stratification phenomenon in flow of Maxwell nanomaterial with motile gyrotactic microorganisms in the presence of magnetic field, Int. J. Mech. Sci. 132 (2017) 426–434.
[45] M.S. Abel, J.V. Tawade, M.M. Nandeppanavar, MHD flow and heat transfer for the upper-convected Maxwell fluid over a stretching sheet, Meccanica 47 (2012) 385–393.
[46] A.M. Megahed, Variable fluid properties and variable heat flux effects on the flow and heat transfer in a non-Newtonian Maxwell fluid over an unsteady stretching sheet with slip velocity, Chin. Phys. B 22 (2013), 094701.
[47] K. Sadeghy, H. Hajibeygi, S.M. Taghavia, Stagnation-point flow of upper-convected Maxwell fluids, Int. J. Nonlinear Mech. 41 (2006) 1242–1247.
[48] S. Mukhopadhyay, Heat transfer analysis of the unsteady flow of a Maxwell fluid over a stretching surface in the presence of a heat source/sink, Chin. Phys. Lett. 29 (2012), 054703.